Available online at www.sciencedirect.com
ScienceDirect
International Journal of Heat and Fluid Flow 28 (2007) 220–228
International Journal of HEAT AND FLUID FLOW
www.elsevier.com/locate/ijhff

Influence of three-dimensional wall roughness on the laminar flow in microtube

Haoli Wang, Yuan Wang *

Department of Fluid Engineering, School of Energy and Power Engineering, Xi'an Jiaotong University, 28 Xianning Western Road, Xi'an, Shaanxi 710049, People's Republic of China

Received 21 July 2005; received in revised form 13 July 2006; accepted 24 August 2006
Available online 21 December 2006

Abstract

The regular perturbation method is introduced to investigate the influences of three-dimensional wall roughness on the laminar flow in microtube. Rough wall surface is modeled by two-dimensional simple harmonic function whose axial and azimuthal wavenumbers are alterable. Under this rough wall model, a set of coupled leading-order and first-order perturbation equations are obtained and computed iteratively. The numerical results show that flow in microtubes are more complex than those in macrotubes; pressure drops are about 0–65% higher than that of Hagen–Poiseuille flow on condition that the relative roughness increases from 0 to 0.05 and the wavenumbers of wall rough function range between 0 and 30; there exists apparent fluctuations in flow fields. Analysis shows that the effects of roughness on the flow pattern is distinct from those on the friction factor.

Keywords: Microtube flow; Three-dimensional wall roughness; Regular perturbation method; Pressure drop; Flow pattern

1. Introduction

Flows in micron-size devices are becoming more prevalent in scientific research and application of multidiscipline. Due to its significance, research of laminar in microchannel has become attractive since early 1980s. However, a strong controversy exists in this research, and inconsistent conclusions have been drawn in many experimental studies. The controversy mainly centers on whether microflow is different from macroflow or not. Some experiments represented great differences between macro- and microflow; whereas some others did not. With respect to these studies, a comprehensive summary was given by Gad-el-Hak (2002), where a number of experimental and numerical studies of microflow are given. Conclusions in quite a number of studies indicate that laminar flow in microchannel have significantly differences from that in macrochannel in terms of friction losses and the flow patterns, and one of the important reasons believed is the influence of the wall roughness on microflow.

Some experiments of the laminar flow in different microchannels with the relative roughness from 0.016 up to 0.05 were implemented by Wu and Little (1983), Mala and Li (1999), Celata et al. (2000), Li et al. (2000), Papautsky et al. (1999) and Jiang et al. (1995). These results indicated that the flow resistances are about 10–90% higher than the theoretical values in the most experiments data, and even a few of them are 350% above the theoretical ones (Wu and Little, 1983). In theoretical and numerical analyses of flows in microchannels, Mala and Li (1999) introduced a roughness viscosity model (RVM) based on the work of Merkle et al. (1974), and this model was implemented to water flows through microtubes and trapezoidal channels, respectively (Qu et al., 2000). Kleinstreuer and Koo (2004) introduced a porous medium layer (PML) mode to simulate several kinds of microscale flow. Wang et al. (2005) introduced a kind of regular perturbation method to study two-dimensional wall roughness on the microscale plane

* Corresponding author. Tel.: +86 29 82663953; fax: +86 29 82668723.
E-mail addresses: whl@cjlu.edu.cn (H. Wang), wangyuan@mail.xjtu.edu.cn (Y. Wang).

0142-727X/$ - see front matter © 2006 Elsevier Inc. All rights reserved.
doi:10.1016/j.ijheatfluidflow.2006.08.005

Nomenclature

A	area of wall surface
C_{mn}	Fourier coefficient
e	inner energy
f	wall rough function
k	iterative index
$\mathbf{n}$	unit normal vector of cross-section
P	pressure
p	pressure oscillation
p_1	first-order pressure oscillation
$\tilde{p}_{mn}$	Fourier coefficients of pressure oscillation
$\widehat{p}_l$	Chebyshev coefficients of pressure
Q	dimensionless flow rate
R	radius of microtube
Re	Reynolds number
S	area of cross-section
S_{ij}	strain rate tensor
$S_{ij}^{(0)}$	leading-order strain rate tensor
$S_{ij}^{(1)}$	first-order strain rate tensor
$\mathbf{u}$	velocity vector
$\mathbf{u}_0$	leading-order perturbation velocity
$\mathbf{U}_0$	apparent leading-order velocity
$\mathbf{u}_1$	first-order perturbation velocity
$\tilde{\mathbf{u}}_{mn}$	Fourier coefficients of velocity
$\widehat{\mathbf{u}}_l$	Chebyshev coefficients of velocity
$U_{\max}$	maximum velocity of tube flow
$\overline{U}$	average velocity of cross-section
r	radial coordinate
x	axial coordinate

Greek symbols

θ	azimuthal coordinate
ε	relative roughness, small parameter
α	axial wavenumber of wall function
β	azimuthal wavenumber of wall function
ξ_j	collocation point
η	ratio of average pressure drop
ρ	fluid density
τ_w	wall shear stress
$\tau_{w,0}$	theoretical wall shear stress
τ_w^*	apparent wall shear stress
Φ	average pressure drop
Φ_0	leading-order average pressure drop
Φ_1	first-order average pressure drop
Θ	viscous dissipation rate
Θ_0	viscous dissipation rate of Hagen–Poiseuille flow, leading-order viscous dissipation rate
Θ_2	second-order viscous dissipation rate
Θ^*	viscous dissipation rate of microtube flow

Operators

D	derivative with respect to r

Poiseuille flow. Hu et al. (2003) numerically simulated laminar flow in rough microtube to study the mechanism of the roughness effect. These theoretical and numerical results show surface roughness has significant effects on both the velocity distribution and the pressure drop.

With respect to the study of the laminar flow in channels with rough wall surfaces, it is a hotspot to use the analytical method. Lesson and Huang (1976) studied the effect of small amplitude wall waviness on laminar boundary layer and the Poiseuille flow in a pipe with axially symmetric wavy walls. The mainly used methods are that of small parameter expansions and Taylor series expansion at rough surface, by which a rough surface is converted into a smooth one. Analysis shows that the apparent slip flow appears over the smooth surface. Hocking (1976) studied the effect of roughness on flow and derived a slip coefficient by using conformal mapping techniques. Jansons (1988) gave a perfect slip microscopic boundary condition of flowing over a randomly rough surface. Michael and Stephen (1994) derived the slip coefficients of flowing over rough surface for single phase flow and one fluid flowing over a coated surfaces by using method of matched asymptotic. Tuck and Kouzoubov (1995) gave a modified slip boundary condition to represent the effects of small roughness-like perturbations to an otherwise-plane fixed wall which is acting as a boundary to steady laminar flow of a viscous fluid. Cable et al. (2002) applied the domain transformation method (DTM) to study the influence of corrugated wall on laminar flow pattern and flow instability between two plates.

So far, most of the theoretical and numerical studies are limited to two-dimensional problems of wall roughness. Due to its complexity, the problem of flow in microflow with three-dimensional rough wall is seen singularly in previous research. However, it is more important to study the influence of three-dimensional roughness on flow because the roughness on virtual wall surface is three-dimensional. Since the relative roughness is believed to be a small parameter in microtube, a regular perturbation method is developed to study the influence of three-dimensional wall roughness on the microtube flow in this study according to Van Dyke (1964). In this method, a rough wall surface is converted into a smooth one and the physical quantities of flow field are expanded into perturbation series. The regular perturbation method was used in other literatures including Lesson and Huang (1976), Töeren (1983), Bontozoglou and Papapolymerou (1996) and Cable et al. (2001) as well as Wang et al. (2005), and so on.

The paper is organized as follows: The mathematical model and numerical method are described in Section 2

where a set of coupled equations are obtained; the solution method for coupled equations is given in Section 3; results and discussion are provided in Section 4 and conclusions are presented in Section 5.

2. Theory

2.1. Perturbation equation

The wall roughness varies irregularly along flow and azimuthal directions but presents the periodic character. For the sake of simplification, wall curved face is assumed to be a two-dimensional periodic function (see Fig. 1), which is called as wall function in this study. Choosing the radius R, the maximum velocity $U_{\max}$ and $\rho U_{\max}^2$ as the characteristic length, velocity and pressure of microtube flow, respectively, the dimensionless continuity equation and time-independent momentum equations of microtube flow are derived and given by Eqs. (1) and (2)

$$\nabla \cdot \mathbf{u} = 0 \tag{1}$$

$$(\mathbf{u} \cdot \nabla)\mathbf{u} = \Phi - \nabla p + Re^{-1}\nabla^2 \mathbf{u} \tag{2}$$

Boundary conditions are bounded at $r = 0$ and no-slip at wall surfaces

$$r = 0, \quad \mathbf{u}, p < \infty \tag{3}$$

$$r = 1 + \varepsilon f(x,\theta), \quad (u,v,w) = \mathbf{0} \tag{4}$$

where u, v, w are the axial, radial and azimuthal velocity components in cylindrical coordinate system, respectively; $\mathbf{\Phi} = (\Phi, 0, 0)$, and Φ the dimensionless averaged pressure drop of laminar flow in microtube; p the pressure oscillation, so the pressure at any a cross-section of flow direction x is $P = P_0 - \Phi\,(x - x_0) + p$, where P_0 is the pressure at initial point of $x = x_0$; ε the small parameter; $f(x,\theta)$ the wall function, and $f(x,\theta) = \mathrm{O}(1)$.

Since the small parameter ε presents in the boundary conditions, all the physical quantities in Eqs. (1) and (2) is decomposed into the perturbation series as Eqs. (5)–(7)

$$\mathbf{u}(x,r,\theta) = \mathbf{u}_0(r) + \varepsilon \mathbf{u}_1(x,r,\theta) + \mathrm{O}(\varepsilon^2) \tag{5}$$

$$p(x,r,\theta) = \varepsilon p_1(x,r,\theta) + \mathrm{O}(\varepsilon^2) \tag{6}$$

$$\Phi = \Phi_0 + \varepsilon \Phi_1 + \mathrm{O}(\varepsilon^2) \tag{7}$$

The boundary conditions at wall surface are expanded to Taylor series at $r = 1$ (Van Dyke, 1964), i.e.

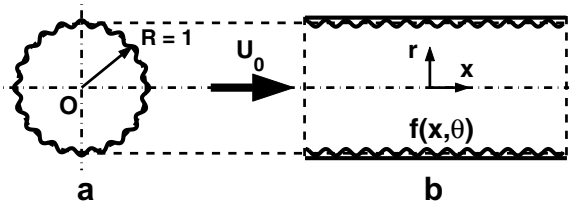

Fig. 1. Schematic of microtube: (a) azimuthal direction, (b) axial direction.

$$\mathbf{u}(x,r,\theta)|_{r=1+\varepsilon f(x,\theta)} = \mathbf{u}(x,1,\theta) + \varepsilon f(x,\theta)\mathbf{u}'(x,1,\theta) + \mathrm{O}(\varepsilon^2) \tag{8}$$

where $\mathbf{u}_0(r) = (u_0(r), 0, 0)$ and $\mathbf{u}_1 = (u_1, v_1, w_1)$ represent the leading-order and the first-order velocities, respectively; Φ_0 the averaged leading-order pressure drop along the flow direction being equal to that of Hagen–Poiseuille flow, and Φ_1 the first-order pressure drop; $(\cdot)'$ denotes the derivative with respect to r.

Substituting Eq. (5) into Eq. (8) and emerging the like terms in ε, we have

$$\mathbf{u}(x,r,\theta)|_{r=1+\varepsilon f(x,\theta)} = \mathbf{u}_0(1) + \varepsilon[\mathbf{u}_1(x,1,\theta) + f(x,\theta)\mathbf{u}_0'(1)] + \mathrm{O}(\varepsilon^2) \tag{9}$$

Substituting Eqs. (5) and (9) into Eqs. (3) and (4), respectively, the boundary conditions at $r = 1$ are derived and given by Eq. (10)

$$r = 1, \quad \mathbf{u}_0 + \varepsilon[\mathbf{u}_1 + f(x,\theta)\mathbf{u}_0'] = 0 \tag{10}$$

Substituting Eqs. (5)–(7) into Eqs. (1) and (2) and emerging the like terms in ε once again, the equations of $\mathbf{u}_0$ and $\mathbf{u}_1$ along with boundary conditions are derived as follows:

$$\frac{1}{r}\frac{\mathrm{d}}{\mathrm{d}r}\left(r\frac{\mathrm{d}u_0}{\mathrm{d}r}\right) = Re\,\Phi_0 \tag{11}$$

$$r = 0, u_0 < \infty; \quad r = 1, \ u_0 = 0 \tag{12}$$

$$\nabla \cdot \mathbf{u}_1 = \mathbf{0} \tag{13}$$

$$(\mathbf{u}_1 \cdot \nabla)\mathbf{u}_0 + (\mathbf{u}_0 \cdot \nabla)\mathbf{u}_1 = \Phi_1 - \nabla p_1 + Re^{-1}\nabla^2 \mathbf{u}_1 \tag{14}$$

$$r = 0, \mathbf{u}_1, p_1 < \infty; \quad r = 1, \quad \mathbf{u}_1 = -f(x,\theta)\mathbf{u}_0' \tag{15}$$

Eq. (11) is that of Hagen–Poiseuille flow, whose dimensionless solution is $u_0 = 1 - r^2$, and accordingly $\Phi_0 \cdot Re = 4$. As the unknown first-order pressure drop, Φ_1, exists in Eq. (14), an approach is applied to deal with Eqs. (11)–(15) as follows: A leading-order velocity, $\mathbf{U}_0 = (U_0, 0, 0)$ (pseudo-velocity), which results in the total averaged pressure drop, Φ, is introduced to substitute the virtual leading-order velocity $\mathbf{u}_0$, and hence Eqs. (11)–(15) can be rewritten as Eqs. (16)–(20)

$$\frac{1}{r}\frac{\mathrm{d}}{\mathrm{d}r}\left(r\frac{\mathrm{d}U_0}{\mathrm{d}r}\right) = -Re\,\Phi \tag{16}$$

$$r = 0, U_0 < \infty; \quad r = 1, \ U_0 = 0 \tag{17}$$

$$\nabla \cdot \mathbf{u}_1 = 0 \tag{18}$$

$$(\mathbf{u}_1 \cdot \nabla)\mathbf{U}_0 + (\mathbf{U}_0 \cdot \nabla)\mathbf{u}_1 = -\nabla p_1 + Re^{-1}\nabla^2 \mathbf{u}_1 \tag{19}$$

$$r = 0, \mathbf{u}_1, p_1 < \infty; \quad r = 1, \quad \mathbf{u}_1 = -f(x,\theta)\mathbf{U}_0' \tag{20}$$

where $\mathbf{u}_1$ is dependent on x, r, θ. It is seen that the parameter Φ_1 is dropped in Eq. (14) and u_0 is replaced by U_0. The velocity U_0 can be expressed as follows:

$$U_0 = u_0(r) + \tilde{u}_0(r) = \frac{\Phi}{\Phi_0}(1 - r^2) = \eta(1 - r^2) \tag{21}$$

where $\tilde{u}_0(r) = (\eta - 1)(1 - r^2)$ is the additional axial velocity determined by the first-order averaged pressure drop

Φ_1; η an undermined coefficient to denote the ratio between the practical pressure drop and the theoretical pressure drop.

Due to the first-order velocity can be considered as periodic disturbance of flow field, the dimensionless flow rate of flow in microtube with three-dimensional roughness satisfies the following relationship:

$$Q = \int_S \mathbf{u}\cdot\mathbf{n}\,\mathrm{d}S = \int_0^1 (1-r^2)2\pi r\,\mathrm{d}r = \frac{\pi}{2} \tag{22}$$

That is to say the first-order velocity satisfies

$$\int_S \mathbf{u}_1\cdot\mathbf{n}\,\mathrm{d}S = 0 \tag{23}$$

where Q is the dimensionless flow rate; S the variable cross-section of rough microtube; $\mathbf{n}$ the unit normal vector of cross-section.

A coupled set of equations in terms of the transformed leading-order velocity and the first-order velocity are given in Eqs. (16)–(20). Solutions for the coupled equations are approached iteratively, and an iterative arithmetic is given in Section 3.

2.2. Solutions for the first-order equations

Wall function $f(x,\theta)$ can be expanded into double Fourier series, whose complex form is as follows:

$$f(x,\theta) = \sum_m \sum_n C_{mn}\exp[\mathrm{i}(m\alpha x + n\beta\theta)] \tag{24}$$

where α and β are the fundamental axial and azimuthal wavenumbers, respectively, α taken as a real, β an integer. As $f(x,\theta)$ is real, $C_{mn} = C^*_{-m,-n}$, where asterisk denotes complex conjugate. The Fourier coefficients C_{mn} are determined by the double integral as Eq. (25)

$$C_{mn} = \frac{1}{A}\int_{-\infty}^{\infty}\int_{-\infty}^{\infty} f(x,\theta)\exp[-\mathrm{i}(m\alpha x + n\beta\theta)]\,\mathrm{d}A \tag{25}$$

The presence of the wall roughness will lead to the disturbance of the flow field inevitably, hence $\mathbf{u}_1$ and p_1 are no other than the first-order response functions, which can be decomposed into Fourier series similar to that of wall function as follows:

$$(\mathbf{u}_1, p_1) = \sum_m \sum_n (\tilde{\mathbf{u}}_{mn}(r), \tilde{p}_{mn}(r))\exp[\mathrm{i}(m\alpha x + n\beta\theta)] \tag{26}$$

where $(\tilde{\mathbf{u}}_{mn}, \tilde{p}_{mn}) = (\tilde{u}_{mn}, \mathrm{i}\tilde{v}_{mn}, \tilde{w}_{mn}, \tilde{p}_{mn})$ are the amplitude functions of velocity and pressure with respect to the radius, respectively.

Chebyshev collocation method is applied to solve the disturbance equations in this study. This method is a high-accuracy numerical method, and the grids can be automatically refined near wall. By using it, the disturbed velocity and pressure are decomposed in spectral space at Chebyshev collocation points as Eq. (27)

$$(\mathbf{u}_1, p_1) = \sum_{|m|\leqslant M}\sum_{|n|\leqslant N}\sum_{0\leqslant l\leqslant J} (\widehat{\mathbf{u}}_{mnl}, \widehat{p}_{mnl}) \times \exp[\mathrm{i}(m\alpha x + n\beta\theta)]T_l(\xi(r)) \tag{27}$$

where $\widehat{\mathbf{u}}_{mnl} = (\widehat{u}_{mnl}, \mathrm{i}\widehat{v}_{mnl}, \widehat{w}_{mnl})$; $T_l(\xi) = \cos(l\arccos\xi)$, $(-1<\xi<1)$ the l-order Chebyshev polynomial, where ξ is evaluated at the Gauss–Lobatto collocation points as Eq. (28)

$$\xi_j = \cos(\pi j/J) \quad (j = 0,1,\ldots,J) \tag{28}$$

where J is the number of collocation points. By the transform of $r = (1-\xi)/2$ according to Khorrami et al. (1989), the variable r in physical space is transformed into Chebyshev variable ξ.

In this study, wall functions are taken as two-dimensional harmonic functions given by Eq. (29), and their complex forms are given in Eq. (30)

$$f(x,\theta) = (1/2)\cos(\alpha x + \beta\theta) \tag{29}$$

$$f(x,\theta) = (1/4)\exp[\mathrm{i}(\alpha x + \beta\theta)] + \mathrm{C.C.} \tag{30}$$

where C.C. denotes the complex conjugate. In this way, the relative roughness being the difference between peak and trough of the wall function is equal to the small parameter ε.

According to Eq. (27), the first-order disturbed velocity and pressure have the forms as Eq. (31)

$$(\mathbf{u}_1, p_1) = (\tilde{\mathbf{u}}_1(r), \tilde{p}_1(r))\exp[\mathrm{i}(\alpha x + \beta\theta)] + \mathrm{C.C.} \tag{31}$$

Notice that boundary conditions at $r = 0$ of Eq. (20) is the singular point of Eq. (19) under cylindrical coordinate system. The explicit expression can be derived according to Khorrami et al. (1989) as follows:

$$\tilde{u}_1(0) = \tilde{v}_1(0) = \tilde{w}_1(0) = \tilde{p}_1(0) = 0 \tag{32}$$

Following Khorrami et al. (1989), the boundary condition of $\tilde{p}$ at $r = 1$ is determined by the equation of the first-order radial velocity as Eq. (33)

$$r = 1, \quad \frac{\mathrm{d}\tilde{p}_1}{\mathrm{d}r} = \frac{1}{Re}\left[\frac{1}{r}\frac{\mathrm{d}}{\mathrm{d}r}\left(r\frac{\mathrm{d}\tilde{v}_1}{\mathrm{d}r}\right)\right] \tag{33}$$

The detailed derivations of Eqs. (32) and (33) can be seen in Appendix.

Substituting Eqs. (31)–(33) into Eqs. (18)–(20), the first-order equations and their boundary conditions are converted into those in spectral space. The discretized equations at collocation points have total $4J+4$ unknown quantities.

3. Solution for the coupled equations

The energy losses of microtube flows are greater than those of flows in tubes with flat walls due to the presences of the wall roughness. Based on this point, the friction loss or pressure drop can be analyzed by energy losses. The dimensionless energy equation of the incompressible flow without internal heat source and heat transfer at the boundary is derived as Eq. (34)

$$\frac{De}{Dt} = Re^{-1}\Theta \tag{34}$$

where e is the dimensionless inner energy (the characteristic energy is taken as U_{max}^2); Θ the dimensionless viscous dissipation rate.

From Eq. (29) we can see that for the incompressible Newtonian fluid, the change rate of inner energy is absolutely contributed by the energy dissipation rate, Θ. For a laminar flow in macrotube, friction loss absolutely results from the wall shear stress, which can be proved by the viscous dissipation being equal to the work of wall shear stress according to Batchelor (1967) as follows:

$$\Theta = \tau_w A\overline{U} \tag{35}$$

where τ_w is shear stress of wall surface, which is in proportion to velocity gradient at wall; A the surface area; $\overline{U}$ the average velocity on cross-section of microtube. Dimensionless wall shear stress of smooth pipe flow is denoted by $\tau_{w,0}$, and $\tau_{w,0} = 1/Re \cdot (du_0/dr) = -2/Re$.

Although there exits different cases of viscous dissipation for the microtube flow, Eq. (35) is also applicable to the flow in microtube with rough wall. Due to surface area and flow rate are invariable for the flow in rough microtube according to perturbation method, we can find an equivalent shear stress τ_w^* resulting in the virtual viscous dissipation. In fact, the equivalent shear stress is in proportion to the gradient of U_0 at $r = 1$. Dimensionless wall shear stress $\tau_w^* = 1/Re \cdot (dU_0/dr) = \eta\tau_{w,0}$.

For an incompressible Newtonian fluid, the total dimensionless viscous dissipation rate within a given area (a periodic area of flow, say) is computed according to Eq. (36) (using the subscript notation)

$$\Theta = -\frac{1}{Re}\int_V (S_{ij}S_{ij})\,dV \quad (i,j = 1,2,3) \tag{36}$$

where V is the volume of the flow area; Θ the total dimensionless viscous dissipation rate; S_{ij} the dimensionless strain rate tensors, which are calculated according to Eq. (37)

$$\begin{aligned} &S_{xx} = \frac{\partial u}{\partial x}, \quad S_{rr} = \frac{\partial v}{\partial r}, \quad S_{\theta\theta} = \frac{1}{r}\frac{\partial w}{\partial \theta} + \frac{v}{r}, \quad S_{xr} = \frac{1}{2}\frac{\partial v}{\partial x} + \frac{1}{2}\frac{\partial u}{\partial r} \\ &S_{\theta x} = \frac{1}{2r}\frac{\partial u}{\partial \theta} + \frac{1}{2}\frac{\partial w}{\partial x}, \quad S_{r\theta} = \frac{r}{2}\frac{\partial}{\partial r}\left(\frac{w}{r}\right) + \frac{1}{2r}\frac{\partial v}{\partial \theta} \end{aligned} \tag{37}$$

From perturbation method, we can obtain the viscous dissipation of flow in rough microtube, Θ^*, by the perturbation expansion, i.e.

$$\begin{aligned} \Theta^* &= -\frac{1}{Re}\int_V \left(S_{ij}^{(0)} + \varepsilon S_{ij}^{(1)}\right)\left(S_{ij}^{(0)} + \varepsilon S_{ij}^{(1)}\right)dV \\ &= -\frac{1}{Re}\left[\int_V \left(S_{ij}^{(0)}S_{ij}^{(0)}\right)dV + \varepsilon^2\int_V \left(S_{ij}^{(1)}S_{ij}^{(1)}\right)dV\right] \\ &= \Theta_0 + \varepsilon^2\Theta_2 \end{aligned} \tag{38}$$

where $S_{ij}^{(0)}$ and $S_{ij}^{(1)}$ are the leading-order and the first-order strain rates, respectively; Θ_0 and Θ_2 the leading-order and the second-order viscous dissipation, respectively. The integral $\int_V \left(S_{ij}^{(0)}S_{ij}^{(1)}\right)dV = 0$ is included in the derivation because $S_{ij}^{(0)}S_{ij}^{(1)}$ are disturbance quantities.

According to Eqs. (36) and (37), dimensionless viscous dissipation rate of Hagen–Poiseuille flow, Θ_0, and that of the laminar flow in microtube, Θ^*, are given in Eqs. (39) and (40), respectively

$$\Theta_0 = -\frac{1}{Re}\int_V \left(\frac{du_0}{dr}\right)^2 dV \tag{39}$$

$$\begin{aligned} \Theta^* = -\frac{2}{Re}\int_V \Bigg\{ &\left(\varepsilon\frac{\partial u_1}{\partial x}\right)^2 + \left(\varepsilon\frac{\partial v_1}{\partial r}\right)^2 + \left(\frac{\varepsilon}{r}\right)^2\left(\frac{\partial w_1}{\partial \theta} + v_1\right)^2 \\ &+ \frac{1}{2}\left(\frac{du_0}{dr} + \varepsilon\frac{\partial u_1}{\partial r} + \varepsilon\frac{\partial v_1}{\partial x}\right)^2 + \frac{\varepsilon^2}{2}\left(\frac{1}{r}\frac{\partial u_1}{\partial \theta} + \frac{\partial w_1}{\partial x}\right)^2 \\ &+ \frac{\varepsilon^2}{2}\left[r\frac{\partial}{\partial r}\left(\frac{w_1}{r}\right) + \frac{1}{r}\frac{\partial v_1}{\partial \theta}\right]^2\Bigg\} dV \end{aligned} \tag{40}$$

Notice that $r = 0$ is a singular point for the third, the fifth and the sixth terms of Eq. (40) under cylindrical coordinate system, we have the following transformations according to the L'Hospital's rule,

$$\begin{aligned} &\lim_{r\to 0}\frac{1}{r^2}\left(\frac{\partial w_1}{\partial \theta} + v_1\right) = \left[\frac{1}{2}\frac{\partial^3 w_1}{\partial r^2\partial\theta} + \frac{\partial^2 v_1}{\partial r^2}\right]_{r=0}; \quad \lim_{r\to 0}\frac{1}{r}\frac{\partial u_1}{\partial \theta} = \left[\frac{\partial^2 u_1}{\partial r\partial\theta}\right]_{r=0} \\ &\lim_{r\to 0}\left[r\frac{\partial}{\partial r}\left(\frac{w_1}{r}\right) + \frac{1}{r}\frac{\partial v_1}{\partial \theta}\right] = \left[\frac{\partial^2 v_1}{\partial r\partial\theta}\right]_{r=0} \end{aligned} \tag{41}$$

From Eqs. (35), (38) and (39) we have

$$\Theta^* = \tau_w^* A\overline{U} = \eta\tau_w A\overline{U} = -\frac{\eta}{Re}\int_V \left(\frac{du_0}{dr}\right)^2 dV = \eta\Theta_0 \tag{42}$$

where $\eta = 1 + \varepsilon^2\left[\int_V \left(S_{ij}^{(1)}S_{ij}^{(1)}\right)dV \Big/ \int_V \left(\frac{du_0}{dr}\right)^2 dV\right]$.

Hence, to solve the ratio of pressure drop between the laminar flow in microtube and theoretical pressure drop of Hagen–Poiseuille flow can be converted to solve the ratio of total viscous dissipation in a same period, i.e.

$$\eta = \frac{\Phi^*}{\Phi_0} = \frac{\Theta^*}{\Theta_0} \tag{43}$$

Therefore, solutions for the coupled equations of Eqs. (16)–(20) are solved through calculating the first-order velocity $\mathbf{u}_1^{(1)}$ by the leading-order velocity $U_0^{(1)} = u_0$ and calculating the viscous dissipation $\Theta^{*(1)}$ by Eq. (35). And then the correction leading-order velocity $U_0^{(2)}$ and the correction first-order velocity $\mathbf{u}_1^{(2)}$ as well as the correction viscous dissipation rate $\Theta^{*(2)}$ are calculated. The process is repeated until distributions of U_0, $\mathbf{u}_1$ with high accuracy degree are obtained. The convergent criteria in this study is given by Eq. (44)

$$\|\Theta^{*(k+1)} - \Theta^{*(k)}\|/\|\Theta_0\| \leqslant 10^{-6} \tag{44}$$

where the superscript k denotes the iterative index.

Calculations indicate that convergent speeds of the iterative processes are satisfying subject to low and moderate Reynolds number ($Re < 10^3$) and small relative roughness

($\varepsilon < 0.1$). In general, for a smaller relative roughness, *Re* could be fairly large. However, it is difficult to converge for a larger value of *Re* as ε increases, and vice versa. But then the convergent speeds are proved quite rapid in the present investigation due to its moderate parameters ($\varepsilon \leqslant 0.05$, $Re \leqslant 500$). Actually, only through no more than ten iterative steps, the convergent accuracies are reached. Compare with conventional numerical solution, the times for modeling of rough elements and CPU consumptions largely decrease.

4. Results and discussion

All the dimensionless parameters in this study are chosen as follows: (1) relative roughness, ε: 0–0.05; (2) wavenumber, $\alpha = \beta$: 0–30; (3) Reynolds number, *Re*: 1–500. In order to insure the accuracy of computing, number of wall grids is 50×50 and that of collocation points is 100 in this study.

4.1. Influence of wall roughness on flow pattern

It is known that the radial and azimuthal velocities are equal to zero if the roughness being not considered (flow in macrotube, say), so their variations under the condition of microtube without ignoring the wall roughness will reflect intuitively the influence of roughness on the flow. The transmissions of the first-order velocities toward the center of flow field at peak of one rough element can be seen from Figs. 2–4.

Fig. 2 presents the transmissions of the first-order velocities toward the center of flow field under different relative roughness (0.01, 0.03 and 0.05) as spatial wavenumber of wall function and Reynolds number are fixed (5 and 100, respectively). The results show that larger relative roughness will have more important influence on flow field due to the fact that amplitude values of all physical quantities

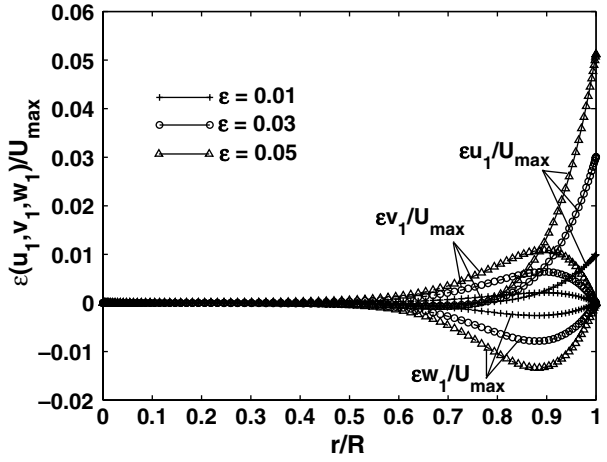

Fig. 2. Transmissions of the first-order velocities toward the center of flow field at peaks of rough elements under different relative roughness ($\alpha = \beta = 5$, $Re = 100$).

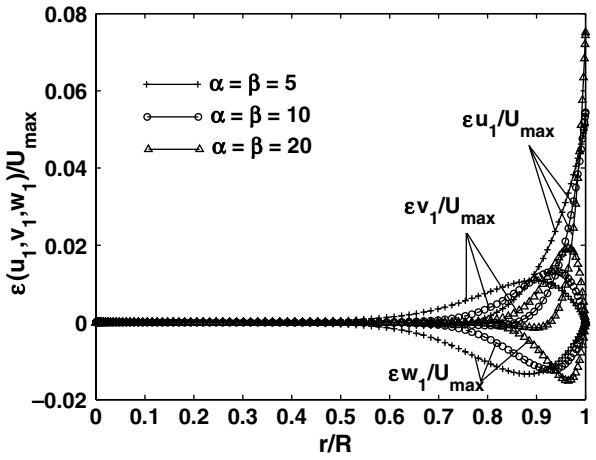

Fig. 3. Transmissions of first-order velocities toward the center of flow field peaks of rough elements under different axial and azimuthal wavenumber ($\varepsilon = 0.05$, $Re = 100$).

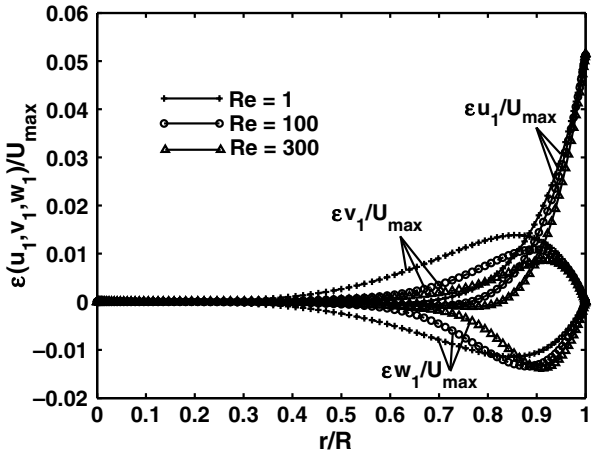

Fig. 4. Transmissions of first-order velocities toward the center of flow field at peaks of rough elements under different Reynolds number ($\varepsilon = 0.05$, $\alpha = \beta = 5$).

increase. As the relative roughness altering from 0.01 to 0.05, the disturbed velocities are extended to a certain area of flow field from wall (nearby $r = 0.5$ for this case, say), and the disturbed areas are invariable. Except the first-order axial velocity, the maximum amplitude values of another two components of velocity present at a certain position in flow field ($r = 0.88$ for this case), where the disturbances are the most intensity. We can see that axial velocity at wall is nonzero, which results from Taylor series expansion of axis velocity at $r = 1$. Furthermore, it can be seen that nonzero axial velocity at computational wall increases with increase of relative roughness, which indicates that the magnitude of this nonzero velocity reflects the disturbance intensity of flow field.

Fig. 3 presents the transmissions of the first-order velocities toward the center of flow field under different spatial wavenumbers on condition that the relative roughness and Reynolds number are fixed (0.05 and 100,

respectively). Altering the wavenumber of wall function implies altering the areal density of rough elements on the wall surface, and the increase of wavenumber leads to that of areal density of rough elements. Notice that the disturbed areas of flow field decrease with the increase of spatial wavenumber, and appearance positions of the maximum amplitude value of disturbed quantities tend to near wall. The reason for this is owing to that the average kinetic energy of main flow increases with the increase of areal density, so that the disturbances are more difficult to transmit toward the center of flow field. We can see from the figures that greater wavenumber of wall function will results in greater nonzero velocity at computational wall, which indicates that the disturbance intensifies under the condition of greater wavenumber.

Fig. 4 presents the transmissions of the first-order velocities toward the center of flow field under different Reynolds number when the relative roughness and wavenumber of wall function are fixed (0.05 and 5, respectively). Notice that the disturbed areas of flow field decrease with the increase of Reynolds number, and appearance positions of maximum amplitude values of the disturbed radial and azimuthal velocities tend to the wall. This can be explained that the increase of Reynolds number will lead to the increase of the average kinetic energy of the main flow so that the effect of wall roughness on the flow pattern will be weakened.

4.2. Influence of wall roughness on pressure drop

Figs. 5–7 present the influences of wall roughness on the pressure drop in terms of relative roughness, wavenumber of wall function and Reynolds number, respectively. It can be seen from Figs. 5 and 6 that the pressure drop will increase from 0% to over 65% higher than the theoretical pressure drop with increase of relative roughness from $\varepsilon = 0$ to $\varepsilon = 0.05$ and wavenumber of wall function from $\alpha = \beta = 0$ to $\alpha = \beta = 30$, which agree well with the experimental results mentioned at the beginning of this paper. The reasons for the influence of relative roughness on the pressure drop can be explained that the higher relative roughness will lead to higher disturbance of flow and therefore give rise to higher viscous dissipation. The reasons for higher wavenumber resulting in higher pressure drop can be ascribed to the fact that the more strong shearing action forms in the flow field due to the increment of disturbance frequency per unit length in the flow direction. Fig. 7 illustrates that the pressure drop increases in some extent with increment of Reynolds number from 1 to 500 under condition of $\varepsilon = 0.05$ and $\alpha = \beta = 5$. The pressure drop of microtube with three-dimensional rough element is found to be 3–4.2% above the theoretical value of Hagen–Poiseuille flow. All the differences are tiny and can be ignored seemingly. However, due to high computational accuracy of Chebyshev spectral collocation method, the computational results can get to at least 7-digit accuracy when the collocated points are taken as more than 52 (see Zhou and Zhao, 2004). In this study, the numerical results are high

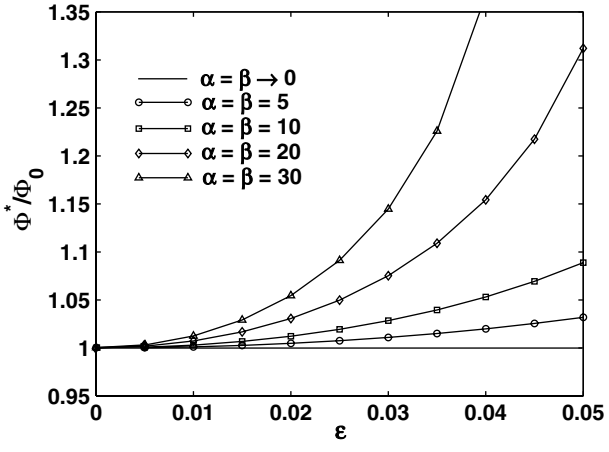

Fig. 5. Variations of the ratio of pressure drop with respect to the relative roughness ($Re = 100$).

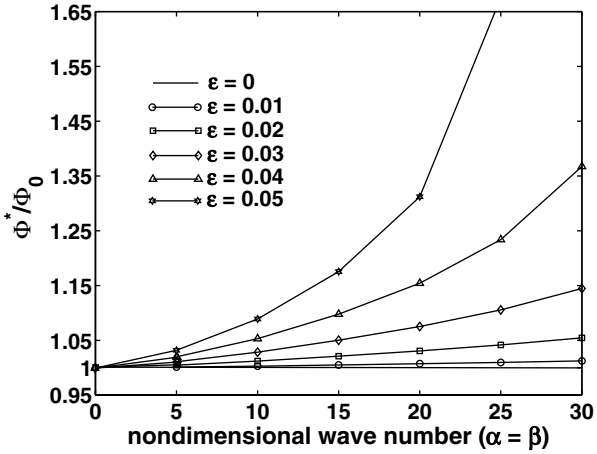

Fig. 6. Variations of the ratio of pressure drop with respect to the wavenumber of wall function ($Re = 100$).

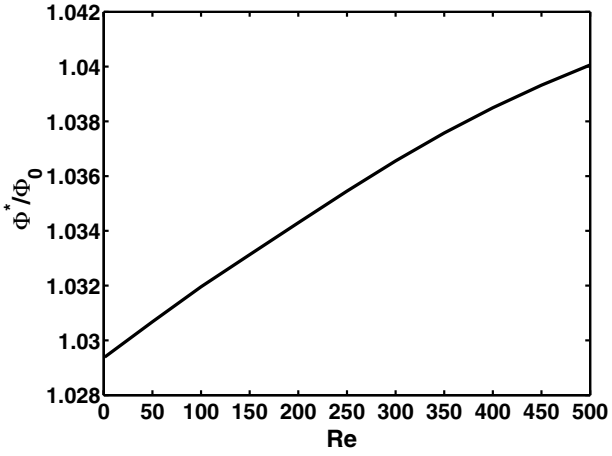

Fig. 7. Variations of the ratio pressure drop with respect to Reynolds number ($\varepsilon = 0.05$, $\alpha = \beta = 5$).

accuracy due to the collocation points are taken as 100, so the differences between computational results and theoretical value of pressure drop do not result from computational errors, but really exist. This implies that the product between pressure drop and Reynolds number of laminar flow in rough microtube has deviated from that of theoretical value of pipe flow.

A group of notable experiments used sand-grains and pipes of different diameter to vary the relative roughness were investigated by Nikuradse (1933), and experimental results indicated that pressure drop is independent of the relative roughness in laminar region. We can see, however, there exists inconsistent conclusions in this paper. The reason for this is not very clear at present, but it is believed for the moment that the influence factors in experiments are more complex than those in the theoretical analysis, by which the influence of single factor can be presented in detail.

5. Conclusions

Perturbation method is an effective method to study the influence of three-dimensional wall roughness on the microtube flow. In this study, the wall roughness curved faces are modeled by two-dimensional harmonic functions and the perturbation equations are derived. A set of coupled equations composed by the leading-order and first-order perturbation equations due to the unknown dimensionless pressure drop are obtained and an iterative arithmetic is given. Applying the spectral collocation method, the first-order perturbation equations are solved numerically. Analytical and computational results show that wall relative roughness, wavenumber of wall rough function as well as Reynolds number are important factors to influence the flow patterns and pressure drop.

If wavenumber of rough function or Reynolds number decreases, the disturbed areas of flow field are larger. The variation of disturbed area is independent of the variation of relative roughness if the relative roughness is a small quantity. The dimensionless pressure drop increases with the increase of relative roughness, Reynolds number or wavenumber of wall function. These results indicate that the influences of wall roughness on the flow pattern are different from those on the pressure drop. The reason is that the influences of roughness on flow pattern depend on the kinetic energy of main flow, whereas the influences of roughness on the pressure drop depend on the energy dissipation of fluid. A conclusion can be drawn from this study that the effect of roughness should not be ignored unless the relative roughness is less than 1%.

Acknowledgement

The authors want to express their gratitude to the Chinese Research Fund for Doctoral Program of Higher Education (No. 20030698004).

Appendix

All the physical quantities are single-valued, smooth and bounded at $r = 0$, so we have

$$\lim_{r\to 0}\frac{\partial \mathbf{u}}{\partial\theta} = 0, \quad \lim_{r\to 0}\frac{\partial p}{\partial\theta} = 0 \tag{A.1}$$

where $\mathbf{u}$ is the total velocity, i.e. $\mathbf{u} = \mathbf{u}_0(r) + \varepsilon\mathbf{u}_1(x, r, \theta) + \mathrm{O}(\varepsilon^2)$. Because the leading-order velocity is only the function with respect to r, we have $\partial\mathbf{u}/\partial\theta = \partial\mathbf{u}_1/\partial\theta$. The total velocity in (A.1) can be written as follows:

$$\lim_{r\to 0}\frac{\partial}{\partial\theta}(u_1\mathbf{e}_x + v_1\mathbf{e}_r + w_1\mathbf{e}_\theta) = 0 \tag{A.2}$$

where $\mathbf{e}_x$, $\mathbf{e}_r$, $\mathbf{e}_\theta$ are unit vectors in flow, radial and azimuthal directions under cylindrical coordinate system, respectively.

Again, $\frac{\partial \mathbf{e}_x}{\partial\theta} = 0, \frac{\partial \mathbf{e}_r}{\partial\theta} = \mathbf{e}_\theta, \frac{\partial \mathbf{e}_\theta}{\partial\theta} = -\mathbf{e}_r$, and substituting them into (A.2), we have

$$\lim_{r\to 0}\frac{\partial \mathbf{u}}{\partial\theta} = \mathrm{i}\beta\tilde{u}_1\mathbf{e}_x - (\beta\tilde{v}_1 + \tilde{w}_1)\mathbf{e}_r + (i\tilde{v} + \mathrm{i}\beta\tilde{w}_1)\mathbf{e}_\theta = \mathbf{0} \tag{A.3a}$$

$$\lim_{r\to 0}\frac{\partial p}{\partial\theta} = \mathrm{i}\beta\tilde{p}_1 = \mathbf{0} \tag{A.3b}$$

Hence, we have

$$\beta\tilde{u}_1 = \beta\tilde{v}_1 + \tilde{w}_1 = \beta\tilde{w}_1 + \tilde{v}_1 = \beta\tilde{p}_1 = 0 \tag{A.4}$$

There are different implements for different values of β as follows:

$$\beta = 0, \quad \tilde{u}_1(0), \quad \tilde{p}_1(0) < \infty, \quad \tilde{v}_1(0) = \tilde{w}_1(0) = 0 \tag{A.5a}$$

$$\beta = \pm 1, \quad \tilde{u}_1(0) = \tilde{p}_1(0) = 0, \quad \tilde{v}_1(0) \pm \tilde{w}_1(0) = 0 \tag{A.5b}$$

$$|\beta| > 1, \quad \tilde{u}_1(0) = \tilde{v}_1(0) = \tilde{w}_1(0) = \tilde{p}_1(0) = 0 \tag{A.5c}$$

Due to $|\beta| > 1$ in this study, the cases of (A.5c) are the boundary conditions at $r = 0$.

The equation of the first-order radial velocity is expanded as Eq. (A.6)

$$\frac{\mathrm{d}\tilde{p}_1}{\mathrm{d}r} = -\mathrm{i}\alpha U_0\tilde{v}_1 + \frac{1}{Re}\left\{\left[\frac{1}{r}\frac{\mathrm{d}}{\mathrm{d}r}\left(r\frac{\mathrm{d}}{\mathrm{d}r}\right) - \frac{\beta^2+1}{r^2} - \alpha^2\right]\tilde{v}_1 - \frac{2\mathrm{i}\beta}{r^2}\tilde{w}_1\right\} \tag{A.6}$$

Since $\tilde{v}_1(1) = \tilde{w}_1(1) = 0$ owing to no-slip conditions, the boundary condition of $\tilde{p}_1$ at $r = 1$ can be determined as follows:

$$r = 1, \quad \frac{\mathrm{d}\tilde{p}_1}{\mathrm{d}r} = \frac{1}{Re}\left[\frac{1}{r}\frac{\mathrm{d}}{\mathrm{d}r}\left(r\frac{\mathrm{d}\tilde{v}_1}{\mathrm{d}r}\right)\right] \tag{A.7}$$

References

Batchelor, G.K., 1967. An introduction to Fluid Dynamics. Cambridge University Press.

Bontozoglou, V., Papapolymerou, G., 1996. Laminar film flow down a wavy incline. Int. J. Multiphase Flow 23 (1), 69–79.

Cable, A., Szumbarski, J., Floryan, J.M., 2001. Numerical simulation of flows over corrugated walls. Comput. Fluids 30, 753–776.

Cable, A., Szumbarski, J., Floryan, J.M., 2002. Stability of flow in a wavy channel. J. Fluids Mech. 457, 191–212.

Celata, G.P., Cumo, M., Gulielmi, M., Zummo, G., 2000. Experimental investigation of hydraulic and single phase heat transfer in 0.130 mm capillary tube. Proc. Int. Conf. Heat Transfer and Transport Phenomena in Microscale. Begell House, Inc, New York, Wallingford, UK, pp. 108–113.

Gad-el-Hak, M., 2002. The MEMS Handbook. CRC Press, New York.

Hocking, L.M., 1976. Moving fluid on a rough surface. J. Fluid Mech. 76, 801–817.

Hu, Y.D., Werner, C., Li, D.Q., 2003. Influence of three-dimensional roughness on pressure-driven flow through microchannels. J. Fluids Eng. 125, 871–879.

Jansons, K.M., 1988. Determination of the macroscopic (partial) slip boundary condition for a viscous flow over a randomly rough surface with a perfect slip microscopic boundary condition. Phys. Fluids 31 (1), 15–17.

Jiang, X.N., Zhou, Z.Y., Yao, J., Li, Y., Ye, X.Y., 1995. Micro-fluid flow in microchannel. Transducers'95, Stockholm, Sweden, June 25–29, pp. 317–320.

Khorrami, M.R., Malik, M.R., Ash, R.L., 1989. Application of spectral collocation techniques to the stability of swirling flows. J. Comp. Phys. 81, 206–229.

Kleinstreuer, C., Koo, L., 2004. Computational analysis of wall roughness effects for liquid flow in micro-conduits. J. Fluids Eng. 126 (1), 1–9.

Lesson, M., Huang, P.S., 1976. Poiseuille flow in a pipe with axially symmetric wavy walls. Phys. Fluids 19 (7), 945–950.

Li, Z.X., Du, D.X., Guo, Z.Y., 2000. Experimental study on flow characteristics of liquid in circular microtubes. In: Proceedings of the International conference on Heat Transfer and Transport Phenomena in Microscale, Ban, Canada, pp. 162–167.

Mala, G.M., Li, D.Q., 1999. Flow characteristics of water in microtubes. Int. J. Heat Fluid Flow 20, 142–148.

Merkle, C.L., Kubota, T., Ko, D.R.S., 1974. An Analytical Study of the Effects of Surface Roughness on Boundary-layer Transition. AF OÅce of Scien. Res. Space and Missile Sys. Org., AD/A004786.

Michael, J.M., Stephen, H.D., 1994. Slip over rough and coated surface. J. Fluid Mech. 273, 801–817.

Nikuradse, J., 1933, Laws of flow in rough pipes. NACA Technical Memorandum 1292.

Papautsky, I., Brazile, J., Ameel, T., Frazier, A.B., 1999. Laminar fluid behavior in microchannels using micropolar fluid theory. Sens. Actuators A 73 (2), 101–108.

Qu, W.L., Mala, G.M., Li, D.Q., 2000. Pressure-driven water flows in trapezoidal silicon microchannels. Int. J. Heat Mass Transfer 43, 353–364.

Töeren, H., 1983. Drag on eccentrically positioned spheres translating and rotating in tubes. J. Fluid Mech. 129, 77–90.

Tuck, E.O., Kouzoubov, A., 1995. A laminar roughness boundary condition. J. Fluid Mech. 300, 59–70.

Van Dyke, M., 1964. Perturbation Methods in Fluid Mechanics. Academic Press, New York.

Wang, H.L., Wang, Y., Zhang, J.Z., 2005. Influence of ribbon structure rough wall on the microscale Poiseuille flow. J. Fluids Eng. 127, 1140–1145.

Wu, P.Y., Little, W.A., 1983. Measurement of friction factors for the low of gases in very fine channels used for microminiature Joule–Thomson refrigerators. Cryogenics 23 (5), 273–277.

Zhou, H., Zhao, G.F., 2004. Hydrodynamic Stability. National Defence Industry Press, Peking (in Chinese).